PALACKÝ UNIVERSITY OLOMOUC

FACULTY OF SCIENCE

Department of Optics

Collective spin operators

DIPLOMA THESIS

Šimon Bräuer

2019

UNIVERZITA PALACKÉHO V OLOMOUCI

PŘÍRODOVĚDECKÁ FAKULTA

Katedra Optiky

Kolektivní spinové operátory

DIPLOMOVÁ PRÁCE

Šimon Bräuer

2019

PALACKÝ UNIVERSITY OLOMOUC
FACULTY OF SCIENCE

Department of Optics

Collective spin operators

DIPLOMA THESIS

Author:	Šimon Bräuer
Study programme:	N1701 Physics
Field of study:	Optics and Optoelectronics
Form od study:	Full-time
Supervisor:	Prof. RNDr. Tomáš Opatrný, Dr.
Co-supervisor:	Mgr. Jan Provazník

UNIVERZITA PALACKÉHO V OLOMOUCI

PŘÍRODOVĚDECKÁ FAKULTA

Katedra Optiky

Kolektivní spinové operátory

DIPLOMOVÁ PRÁCE

Vypracoval:	Šimon Bräuer
Studijní program:	N1701 Fyzika
Studijní obor:	Optika a optoelektronika
Forma studia:	prezenční
Vedoucí diplomové práce:	Prof. RNDr. Tomáš Opatrný, Dr.
Konzultant diplomové práce:	Mgr. Jan Provazník

Abstract

The aim of this thesis is to explore the possibilities of implementing Hamiltonians acting on collective symmetric spin states of multiatomic sets. If the experiment allows to construct the linear and quadratic functions of the components of the collective spin operator $\hat{J}$, the task is to find out to what extent it is possible to emulate the effects of higher powers of these operators on the system under investigation. In particular, the motivation is the preparation and transformation of quantum states for the purposes of quantum information processing. In the introductory part of the thesis we will analyze the properties of the operator $\hat{J}$ and discuss some important experimental arrangements with regard to the processing of quantum information. In the main part there will be research results focused on possibilities of construction of higher order Hamiltonians and their optimization with respect to number of steps and required accuracy.

Keywords

collective spin operators, cubic nonlinearity,
Q-function, coherent state, squeezed state,
emulation, optimization, quasi-Newton method,
BFGS, asymmetry,
unitary operator, unitary evolution,
quantum computing, qubit, commutator identities

Abstrakt

Cílem této práce je prozkoumat možnosti implementace hamiltoniánů působících na kolektivní symetrické spinové stavy mnohaatomových souborů. Pokud experiment umožňuje konstruovat lineární a kvadratické funkce složek operátoru kolektivného spinu $\hat{J}$, úkolem je zjistit, do jaké míry lze emulovat působení vyšších mocnin těchto operátorů na zkoumaný systém. Motivací je zejména příprava a transformace kvantových stavů pro účely zpracování kvantové informace. V úvodní části diplomové práce bude proveden rozbor vlastností operátoru $\hat{J}$ a prodiskutují se některá důležitá experimentální uspořádání s ohledem na zpracování kvantové informace. V hlavní části pak budou vlastní výzkumné výsledky zaměřené na možnosti konstrukce hamiltoniánů vyšších řádů a jejich optimalizace s ohledem na počet kroků a požadovanou přesnost.

Klíčová slova

kolektivní spinové operátory, kubická nelinearita,
Q-funkce, koherentní stav, stlačený,
emulace, optimalizace, quasi-Newtonova metoda,
BFGS, asymetrie,
unitární operátor, unitární evoluce,
kvantové počítání, qubit, komutační identity

Declaration

I hereby state that I have written Diploma Thesis "Collective spin operators" on my own under the guidance of Prof. RNDr. Tomáš Opatrný, Dr. by using theoretical resources, which are referred to in the list of literature. I agree with the further use of this document according to the requirements of the Department of Optics.

Declared in Olomouc on ....

Contents

List of Figures

Introduction

Clasical computers cursed us with the internet, smarthones and even sent humans to the Moon. But there are many problems too complicated for classical computers; for example simulation of interactions between molecules in quantum chemistry could be performed efficiently using a quantum computer [1].

Let us imagine all kinds of computers of both classical and quantum types. Classical computers are a part of our daily lives. We use digital computers at home, at school, or at work. These are computers that allow us to process data, i.e., logical and numerical values. Another type of computers are analog computers [2, 3]. The idea behind these computers is that using electrical or mechanical systems we can produce an analog of another physical system. So, for example, using a set of electronic components, such as resistors (R), inductors (L) and capacitors (C), we are able to create circuits with behavior corresponding to the behavior of a mechanical oscillator. Thus, in general, we employ these computers to create analogies to other physical systems.

We also have two options to process information in quantum world, the first is to work with discrete variables [4], which technically corresponds to digital computing, and the other is to use continuous variables [4, 5, 6], a regime corresponding to analog computers. With continuous variables we can simulate various continuous quantum systems. Were we able to do this, we would have a universal continuous variable computer.

Nowadays we have a lot of linear operations in quantum physics at our disposal, even in quantum optics. However, by using only these simple operations we are unable to achieve universal computation, even on the polynomial Hamiltonian class [7]. To achieve this we need nonlinear operators such as $\hat{X}^3$. To give a general idea of what a universal computer actually is, we chose 3 key points that Richard Feynman and David Deutsch mentioned [1, 8]. According to them, universal quantum computer is

1. an assembly of independent qubits, each of which functions according to the probabilistic nature of quantum mechanics, including superposition and entanglement of quantum states, as well as a universal quantum logic gate set which supports all of the operations possible at the quantum mechanical level for each qubit,

2. can simulate or implement any and all operations of a classical computer, for example classic Turing machine,

3. and is capable of simulating physics, especially quantum mechanics, but the rest of physics as well.

In this work we will focus on a particular problem in the construction of continuous variable quantum computers. Since we work in continuous variables, we don't have qubits, however, we encode information into continous properties of collective spin systems. In our case we work with squeezed spin states; we need a large amount of these states and we need them to communicate with each other. Furthermore to build an universal quantum computer we need to be able to simulate any Hamiltonian. If we consider a general Hamiltonian in Taylor's expansion, we find linear, quadratic, and higher order terms. The linear and the quadratic terms can be realized in the lab, but to construct higher order terms is a problem. We will tackle a narrow part of this problem by developing operators of cubic nonlinearities.

The goal of this diploma thesis is to find a way to create a cubic operator in the simplest way possible, and to make this procedure experimentally accessible to be one step closer to realizing universal computers. Our procedures are based on collective spins of trapped atoms because nonlinear operations in this media are much more accessible than, for example in quantum optics, where some nonlinear operations like Kerr's nonlinearity are quite inefficient and difficult to achieve.

Chapter I

Theoretical framework

We briefly overview the necessary theoretical framework. We define collective spin and introduce different representations of collective spin operators; we review some of the basic operations and states our work relies on.

1.1 Collective spin operators

The spin $\frac{1}{2}$ of one particle can be described using a set of measurable operators [9]

$$\hat{\sigma}_x = \begin{pmatrix} 0 & 1 \\ 1 & 0 \end{pmatrix}, \quad \hat{\sigma}_y = \begin{pmatrix} 0 & -\imath \\ \imath & 0 \end{pmatrix}, \quad \hat{\sigma}_z = \begin{pmatrix} 1 & 0 \\ 0 & -1 \end{pmatrix} \tag{1.1.1}$$

satisfying the commutation and anti-commutation relations

$$[\hat{\sigma}_i, \hat{\sigma}_j] = 2\imath\epsilon_{ijk}\hat{\sigma}_k, \tag{1.1.2}$$

$$\hat{\sigma}_i\hat{\sigma}_j + \hat{\sigma}_j\hat{\sigma}_i = 0, \quad \text{for } i \neq j. \tag{1.1.3}$$

The operators defined in (1.1.1) are commonly called Pauli operators [9] and correspond to the projection of the spin onto one of the three orthogonal axes (x, y, z). We now consider a system of N particles with spin $\frac{1}{2}$. The collective angular momentum operators are then given by [10]

$$\hat{J}_\alpha = \frac{1}{2}\sum_{l=1}^{N} \hat{\sigma}_{l\alpha}, \quad \alpha = x, y, z \tag{1.1.4}$$

where $\sigma_{l\alpha}$ are the Pauli matrices (1.1.1) for the l-th particle. Alternatively we can employ the Schwinger's representation which allows us to rewrite (1.1.4) in terms of two-mode bosonic system. We consider the $\hat{a}_{1,2}$ and $\hat{a}_{1,2}^\dagger$ operators, where $\hat{a}_i$ ($\hat{a}_i^\dagger$) annihilates (creates) an atom in state $|g_i\rangle$ ($|e_i\rangle$). These operators satisfy the bosonic commutation rules

$$\left[\hat{a}_i, \hat{a}_j^\dagger\right] = \delta_{ij}. \tag{1.1.5}$$

We then proceed to define the angular momentum operators $\hat{J}_x$, $\hat{J}_y$ and $\hat{J}_z$ as

$$\hat{J}_x = \frac{1}{2}(\hat{a}_1^\dagger \hat{a}_2 + \hat{a}_1 \hat{a}_2^\dagger),$$
$$\hat{J}_y = \frac{1}{2\imath}(\hat{a}_1^\dagger \hat{a}_2 - \hat{a}_1 \hat{a}_2^\dagger), \tag{1.1.6}$$
$$\hat{J}_z = \frac{1}{2}(\hat{a}_1^\dagger \hat{a}_1 - \hat{a}_2^\dagger \hat{a}_2),$$

satisfying the commutation relations similar to (1.1.2) based on (1.1.4)

$$\left[\hat{J}_k, \hat{J}_l\right] = \imath\epsilon_{klm}\hat{J}_m, \quad k,l,m \in \{x,y,z\}. \tag{1.1.7}$$

We can also define the operator of total number of atoms

$$\hat{N} = \hat{a}_1^\dagger \hat{a}_1 + \hat{a}_2^\dagger \hat{a}_2 \tag{1.1.8}$$

satisfying relation

$$\hat{J}^2 = \hat{J}_x\hat{J}_x + \hat{J}_y\hat{J}_y + \hat{J}_z\hat{J}_z = \frac{\hat{N}}{2}\cdot\left(\frac{\hat{N}}{2}+1\right). \tag{1.1.9}$$

1.2 Linear and quadratic operations

We will introduce basic operations at most quadratic Hamiltonians in terms of $\hat{J}_i$. The unitary operator corresponding to the linear Hamiltonian

$$\hat{U}_{\text{rot}}(\beta) = e^{\imath \hat{J}_i \beta}, \tag{1.2.1}$$

essentially rotates the spin state around some axis. Here i corresponds to x, y, z axes and β gives the angle of rotation. It is possible to write in a completely general form

$$\hat{U}_{\text{rot}_{\text{gen}}}(\vec{\Omega}) = e^{\imath\left(\hat{J}_x\Omega_x + \hat{J}_y\Omega_y + \hat{J}_z\Omega_z\right)}. \tag{1.2.2}$$

Similarly the unitary operator corresponding to the quadratic Hamiltonian [11] it can be generally defined in shape

$$\hat{U}_{\text{quadratic}_{\text{gen}}}(\chi,\tau) = e^{\imath\sum_{j,k}\chi_{jk}\hat{J}_j\hat{J}_k\tau}, \quad j,k \in \{x,y,z\}, \tag{1.2.3}$$

here χ_{jk} are components which gives the strength of the non-linearity and τ is the time parameter. But we will be interested in one particular case of a quadratic Hamiltonian

$$\hat{U}_{\text{quadratic}}(\chi,\tau) = e^{\imath\hat{J}_z^2\chi\tau}, \tag{1.2.4}$$

which is called one-axis twisting [12], it is experimentally achievable quadratic operation [13, 14].

1.2.1 Experimental realization

One of the possibe approaches to generating spin dynamics similar to those of the one-axis twisting Hamiltonian $\hat{H} \propto \hat{J}_z^2$ relies on repeated interaction of the atomic ensemble with light circulating in an optical resonator. The atoms of ^{87}Rb are trapped in a standing-wave dipole trap inside of an optical resonator. The probe beam has frequency twice as large as the frequency of the optical trap. The reason is that we need all trapped atoms feel the same maximum field strength.

If we tune frequency halfway between the spin levels g_1, g_2 (figure I.1), we can ideally change the distance of these two levels due to AC Stark effect [15]. Changing the distance of these spin levels results in a change in the effective refractive index of the medium of the optical cavity. By changing the refractive index we control the field strength inside the cavity. Hamiltonian describing field

$$\hat{H} \propto k \cdot \hat{J}_z + \hat{c}^\dagger \hat{c}, \tag{1.2.5}$$

where $\hat{J}_z$ is the difference in the number of particles (1.1.6) in the levels g_1, g_2 , $\hat{c}^\dagger \hat{c}$ corresponds to the intensity of the radiation and k is a radiation dependent parameter. Thus, by changing the refractive index, we increase the intensity, so the parameter k will approach the value of $\hat{J}_z$ and the Hamiltonian becomes $\hat{H} \propto \hat{J}_z^2$.
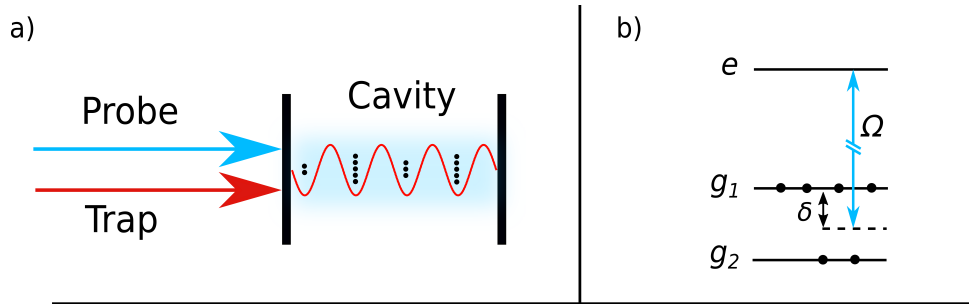
Figure I.1: a) The atoms are trapped in standing-wave dipole trap inside an optical resonator. b) The cavity is tuned halfway between the optical transition frequencies for the two spin states (g_1, g_2).

Other interesting quadratic Hamiltonians we encounter are

$$\hat{U}_{\text{quadratic}_{\text{TA}}}(\chi, \tau) = e^{i(\hat{J}_k \hat{J}_j + \hat{J}_j \hat{J}_k)\chi\tau}, \quad j, k \in \{x, y, z\}, \tag{1.2.6}$$

whose corresponds to the two-axis countertwisting. Possible physical realization of such a Hamiltonian has been studied recently in [16, 17].

Another possible way to form one-axis twisting is through the use of Bose-Einstein condensate with ^{87}Rb [18]. In essence collisions between atoms in dissimilar states differ, leading to $\hat{J}_z^2$ interaction, but alas this method is not reversible.

1.3 Dicke states

Before we define a coherent spin state, we introduce Dicke states. We consider a single particle of spin J and the ground state $|0\rangle$ as the state such that

$$\hat{J}_z |0\rangle = J |0\rangle , \tag{1.3.1}$$

where $\hat{J}_z$ is the operator of the z component of spin. We define a ladder operator [9]

$$\hat{J}_- = \hat{J}_x - \imath \hat{J}_y. \tag{1.3.2}$$

We then have

$$\left(\hat{J}_-\right)^p |0\rangle = \left(\frac{p!2J!}{(2J-p)!}\right)^{\frac{1}{2}} |p\rangle \qquad 0 \leq p \leq 2J \tag{1.3.3}$$

where $|p\rangle$ is the Dicke state and the eigenstate of $\hat{J}_z$ such that

$$\hat{J}_z |p\rangle = (J - p) |p\rangle . \tag{1.3.4}$$

If we consider N two level systems, the dimension of the underlying Hilbert space becomes 2^N. This exponential spatial complexity effectively forbids classical numerical simulations involving larger systems. Under specific circumstances [19, 20] we can get around this issue by introducing so called Dicke states. The spatial complexity then becomes $N + 1$ instead of 2^N. Let us, for example, consider the case of a three particle system ($N = 3$). We consider state with different orientations of spins, either spin up ($\uparrow$) or spin down ($\downarrow$). We have

$$
\begin{aligned}
|0\rangle_D &\propto |\downarrow\downarrow\downarrow\rangle , \\
|1\rangle_D &\propto |\uparrow\downarrow\downarrow\rangle + |\downarrow\uparrow\downarrow\rangle + |\downarrow\downarrow\uparrow\rangle , \\
|2\rangle_D &\propto |\uparrow\uparrow\downarrow\rangle + |\downarrow\uparrow\uparrow\rangle + |\uparrow\downarrow\uparrow\rangle , \\
|3\rangle_D &\propto |\uparrow\uparrow\uparrow\rangle ,
\end{aligned}
\tag{1.3.5}
$$

where $|\cdot\rangle_D$ denotes the Dicke state.

1.4 Coherent spin states

Similar to the defined coherent state of a harmonic oscillator [21, 22], we define a spin coherent state. It is possible to use (1.2.1) to define a coherent state as the ground state rotation

$$|\eta\rangle = \hat{U}_{\mathrm{rot}}(\beta) |0\rangle, \tag{1.4.1}$$

another way to define a coherent state is using a Dicke state (1.3.4)

$$|\eta\rangle = C^{-\frac{1}{2}} \sum_{p=0}^{2J} \left(\frac{2J!}{p!(2S-p)!} \right)^{\frac{1}{2}} \eta^p |p\rangle, \tag{1.4.2}$$

where η runs over the the complex plane and C is a normalization factor. We have

$$\langle \eta | \eta \rangle = C^{-1} \sum_{p=0}^{2J} \frac{2J!}{p!(2S-p)!} |\eta|^{2p} = C^{-1} \left(1 + |\eta|^2 \right)^{2J} \tag{1.4.3}$$

and hence the normalized coherent spin state is

$$|\eta\rangle = \left(1 + |\eta|^2 \right)^{-J} \sum_{p=0}^{2J} \left(\frac{2J!}{p!(2S-p)!} \right)^{\frac{1}{2}} \eta^p |p\rangle. \tag{1.4.4}$$

1.5 Visualization of spin states

Most of our numerical simulation results are presented using Bloch spheres [23] which are a unit 2-spheres, with opposing points corresponding to mutually orthogonal states and others points correspond to the coherent states. The north and south poles of the Bloch sphere are typically chosen to correspond to the standard basis vectors of $\hat{J}_z$, which means spin-up and spin-down states. The points on the surface of the sphere correspond to pure states of the system, whereas the interior points correspond to mixed states, but this applies to a two-level system. In our case, these are N two-level systems, so the Bloch sphere is for us only a geometric figure to which we apply Q-function.
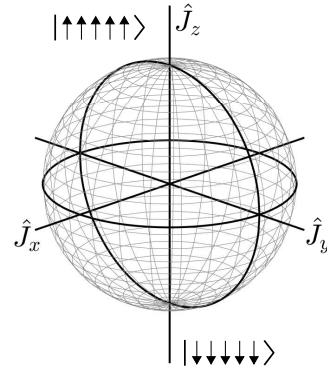

Figure I.2: Picture of the Bloch sphere.

Some results are presented using Hammer's projection [24] of the Bloch sphere, which means projection of three dimensional Bloch sphere into two dimensional space. Using the 2:1 elliptical outer shape as the Mollweide projection, Hammer projection intended to reduce distortion in the

9

regions of the outer meridians, where it is extreme in the Mollweide projection. The longitude and latitudes can then be calculated by

$$\phi = 2\arctan\left(\frac{zx}{2\left(2z^2 - 1\right)}\right),$$

$$\theta = \arcsin(zy),$$

(1.5.1)

where ϕ is the longitude from the central meridian and θ is the latitude. The x, y, z variables are the ellipse coordinates.
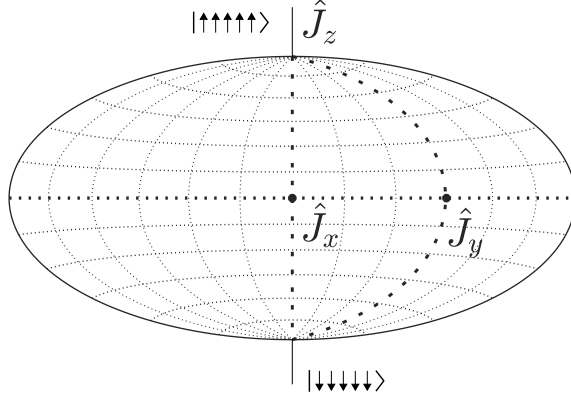
Figure I.3: Picture of the Bloch sphere in the Hammer's projection.

1.6 Husimi Q-function

Instead of describing quantum systems in terms of density matrices we can also employ description using Husimi Q-function [22, 25]:

$$Q(\alpha) = \frac{1}{\pi}\operatorname{tr}\left\{\hat{\rho}\left|\alpha\right\rangle\left\langle\alpha\right|\right\}$$

$$= \frac{1}{\pi}\left\langle\alpha\right|\hat{\rho}\left|\alpha\right\rangle$$

(1.6.1)

where $\hat{\rho}$ is a density matrix, $\left|n\right\rangle$ is a Fock state and $\left|\alpha\right\rangle$ is given by

$$\left|\alpha\right\rangle = e^{\frac{|\alpha|^2}{2}}\sum_{n=0}^{\infty}\frac{\alpha^n}{\sqrt{n!}}\left|n\right\rangle.$$

(1.6.2)

We can adapt the function (1.6.1) defined for harmonic oscillator and analogously obtain

$$Q(\eta) = \frac{1}{\pi}\operatorname{tr}\left\{\hat{\rho}\left|\eta\right\rangle\left\langle\eta\right|\right\}$$

$$= \frac{1}{\pi}\left\langle\eta\right|\hat{\rho}\left|\eta\right\rangle.$$

(1.6.3)

for coherent spin states (1.4.4).

Figure I.4: Visualization of different states using Q-function mapped onto Bloch sphere. a) Coherent spin state. b) Evolution of coherent spin state under (1.2.4) unitary. c) Cubic non-linearity (2.1.5) applied to coherent spin state.

Chapter II

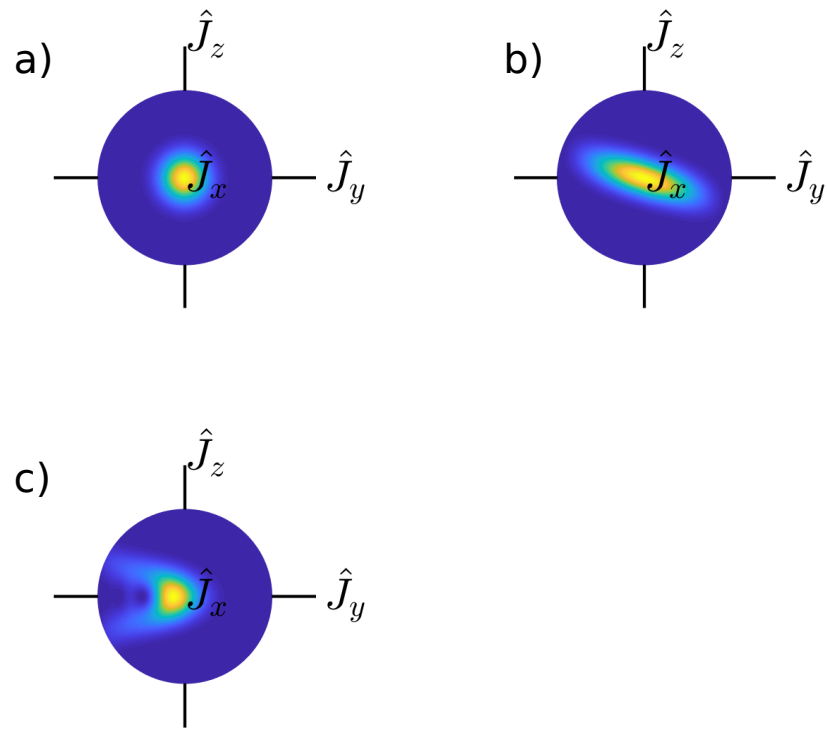# Cubic Hamiltonian for collective spins

It is well known [7] that at least a single non-Gaussian operation is needed to construct universal continous variable quantum computer. In this chapter we review one possible method [26] of creating a cubic nonlinearity in terms of the collective spin operators $\hat{J}_i$. We build on this approach and consequently propose a novel, experimentally feasible procedure.

2.1 Universal procedure

A procedure that equally for all states is considered universal. In our case we are interested in a universal procedure producing a perfect cubic nonlinearity.

It is possible to create higher order polynomials of collective spin operators (1.1.6) using a commutator sequence. This idea was initially developed by Braunstein and Loyd [7] and applied to bosonic harmonic oscillator [7]. It was later extended by Opatrný [26] to collective spin operators and exploited to creat cubic nonlinearity. Opatrný consequently succeeded in finding the sequence

$$
\begin{aligned}
\hat{J}_z^3 = \quad & \frac{\imath}{4} \left[\left(\hat{J}_y^2 - \hat{J}_x^2 \right), \left(\hat{J}_x \hat{J}_y + \hat{J}_y \hat{J}_x \right) \right] + \\
& \frac{\imath}{4} \left[\left(\hat{J}_z \hat{J}_y + \hat{J}_y \hat{J}_z \right), \left(\hat{J}_z \hat{J}_x + \hat{J}_x \hat{J}_z \right) \right] + \frac{1}{4} \hat{J}_z.
\end{aligned}
\tag{2.1.1}
$$

Here the quadratic terms such as $\left(\hat{J}_x \hat{J}_y + \hat{J}_y \hat{J}_x \right)$ appear in each commutator. We would like to propose an experimentally feasible procedure beased on (2.1.1) using only linear and quadratic operators (1.2.1) and (1.2.4) as these linear and quadratic operations are experimentally acces-

sible [27, 28]. With the aid of the commutator identities

$$
\begin{aligned}
[A + B, C] &= [A, C] + [B, C], \\
[A, A] &= 0, \\
[A, B] &= -[B, A], \\
[A, BC] &= [A, B]C + B[A, C],
\end{aligned}
\tag{2.1.2}
$$

and the product relation

$$
\mathrm{e}^{-\imath A \Delta t} \cdot \mathrm{e}^{-\imath B \Delta t} \cdot \mathrm{e}^{\imath A \Delta t} \cdot \mathrm{e}^{\imath B \Delta t} = \mathrm{e}^{[A,B]\Delta t^2} + \mathcal{O}\left(\Delta t^3\right).
\tag{2.1.3}
$$

and with the help of the approximation

$$
\left(\mathrm{e}^{\tau \hat{A}} \cdot \mathrm{e}^{\tau \hat{B}}\right) = \mathrm{e}^{\left(\hat{A}+\hat{B}\right)\tau} + \mathcal{O}\left(\tau^2\right),
\tag{2.1.4}
$$

it is possible to obtain the cubic unitary operator

$$
\hat{U}_{\mathrm{cubic}}(\chi\tau) = \mathrm{e}^{\imath \hat{J}_x^3 \chi\tau}
\tag{2.1.5}
$$

as a sequence of linear and quadratic operators by breaking down the quadratic operators in the commutators in (2.1.1) using (2.1.2), (2.1.3) and (2.1.4)

$$
\mathrm{e}^{\imath\left(\hat{J}_y^2 - \hat{J}_x^2\right)\chi\tau} \approx \mathrm{e}^{\imath \hat{J}_x \frac{\pi}{2}} \cdot \mathrm{e}^{\imath \hat{J}_z^2 \chi\tau} \cdot \mathrm{e}^{-\imath \hat{J}_x \frac{\pi}{2}} \cdot \mathrm{e}^{\imath \hat{J}_y \frac{\pi}{2}} \cdot \mathrm{e}^{-\imath \hat{J}_z^2 \chi\tau} \cdot \mathrm{e}^{-\imath \hat{J}_y \frac{\pi}{2}},
\tag{2.1.6}
$$

$$
\mathrm{e}^{\imath\left(\hat{J}_x \hat{J}_y + \hat{J}_y \hat{J}_x\right)\chi\tau} \approx \mathrm{e}^{-\imath \frac{\pi\sqrt{(2)}}{4}\left(\hat{J}_x - \hat{J}_y\right)} \cdot \mathrm{e}^{\imath\left(\hat{J}_z^2\right)\chi\tau} \cdot \mathrm{e}^{\imath \frac{\pi\sqrt{(2)}}{4}\left(\hat{J}_x - \hat{J}_y\right)} \cdot
$$
$$
\mathrm{e}^{-\imath \frac{\pi\sqrt{(2)}}{4}\left(\hat{J}_x + \hat{J}_y\right)} \cdot \mathrm{e}^{-\imath\left(\hat{J}_z^2\right)\chi\tau} \cdot \mathrm{e}^{\imath \frac{\pi\sqrt{(2)}}{4}\left(\hat{J}_x - \hat{J}_y\right)},
\tag{2.1.7}
$$

$$
\mathrm{e}^{\imath\left(\hat{J}_z \hat{J}_y + \hat{J}_y \hat{J}_z\right)\chi\tau} \approx \mathrm{e}^{\imath \hat{J}_x \frac{\pi}{4}} \cdot \mathrm{e}^{\imath \hat{J}_z^2 \chi\tau} \cdot \mathrm{e}^{-\imath \hat{J}_x \frac{\pi}{4}} \cdot \mathrm{e}^{-\imath \hat{J}_x \frac{\pi}{4}} \cdot \mathrm{e}^{-\imath \hat{J}_z^2 \chi\tau} \cdot \mathrm{e}^{\imath \hat{J}_x \frac{\pi}{4}},
\tag{2.1.8}
$$

$$
\mathrm{e}^{\imath\left(\hat{J}_z \hat{J}_x + \hat{J}_x \hat{J}_z\right)\chi\tau} \approx \mathrm{e}^{-\imath \hat{J}_y \frac{\pi}{4}} \cdot \mathrm{e}^{\imath \hat{J}_z^2 \chi\tau} \cdot \mathrm{e}^{\imath \hat{J}_y \frac{\pi}{4}} \cdot \mathrm{e}^{\imath \hat{J}_y \frac{\pi}{4}} \cdot \mathrm{e}^{-\imath \hat{J}_z^2 \chi\tau} \cdot \mathrm{e}^{-\imath \hat{J}_y \frac{\pi}{4}}.
\tag{2.1.9}
$$

Finally we obtain (2.1.5) in the form of

$$
\begin{aligned}
\hat{U}_{\mathrm{universal}}(\chi\tau) = \;& \mathrm{e}^{-\imath\left(\hat{J}_y^2 - \hat{J}_x^2\right)\sqrt{\chi\tau}} \cdot \mathrm{e}^{-\imath\left(\hat{J}_x \hat{J}_y + \hat{J}_y \hat{J}_x\right)\sqrt{\chi\tau}} \cdot \mathrm{e}^{\imath\left(\hat{J}_y^2 - \hat{J}_x^2\right)\sqrt{\chi\tau}} \cdot \\
& \mathrm{e}^{\imath\left(\hat{J}_x \hat{J}_y + \hat{J}_y \hat{J}_x\right)\sqrt{\chi\tau}} \cdot \mathrm{e}^{-\imath\left(\hat{J}_z \hat{J}_y + \hat{J}_y \hat{J}_z\right)\sqrt{\chi\tau}} \cdot \mathrm{e}^{-\imath\left(\hat{J}_z \hat{J}_x + \hat{J}_x \hat{J}_z\right)\sqrt{\chi\tau}} \cdot \\
& \mathrm{e}^{\imath\left(\hat{J}_z \hat{J}_y + \hat{J}_y \hat{J}_z\right)\sqrt{\chi\tau}} \cdot \mathrm{e}^{\imath\left(\hat{J}_z \hat{J}_x + \hat{J}_x \hat{J}_z\right)\sqrt{\chi\tau}} \cdot \mathrm{e}^{\imath \frac{1}{4}\hat{J}_z \chi\tau},
\end{aligned}
\tag{2.1.10}
$$

which contains 49 linear and quadratic unitary operators from (2.1.6) — (2.1.9). If we look at the relationship between (2.1.5) and (2.1.10), it is as follows

$$
\hat{U}_{\mathrm{cubic}}(\chi\tau) \approx \hat{U}_{\mathrm{universal}}(\chi\tau)
\tag{2.1.11}
$$

which is caused by the used approximations.

13

2.2 Local procedure

Unlike the universal procedure, a local procedure only works with certain states. We are unable to guarantee a perfect outcome for each and every possible state. While this is a significant drawback, giving up universality may have its advantages, such as reduced complexity of all the interactions involved in the procedure.

This approach was discovered during the analysis of the complexity of the cubic operator (2.1.10). We noticed the asymmetrical effects of the unitary operator

$$\hat{U} = \mathrm{e}^{i\left(\hat{J}_x \hat{J}_y + \hat{J}_y \hat{J}_x\right)\tau}. \tag{2.2.1}$$

on squeezed coherent spin states (figure II.1). The effect, demonstrated in the first row of the figure II.1, can be exploited to create a formula emulating the cubic operator (2.1.10) using the experimentally available linear and quadratic operators

$$\begin{aligned}
\hat{U}_{\mathrm{local}}(\alpha_1, \ldots, \alpha_8, t_1, t_2, t_3) &= e^{i\hat{J}_z \alpha_8} \cdot e^{i\hat{J}_x \alpha_7} \cdot \hat{C}(t_3) \cdot \\
&\quad e^{i\hat{J}_z \alpha_6} \cdot e^{i\hat{J}_x \alpha_5} \cdot e^{i\hat{J}_y \alpha_4} \cdot \hat{B}(t_2) \cdot \\
&\quad e^{i\hat{J}_y \alpha_3} \cdot e^{i\hat{J}_z \alpha_2} \cdot e^{i\hat{J}_y \alpha_1} \cdot \hat{A}(t_1),
\end{aligned} \tag{2.2.2}$$

where the expressions $\hat{A}(t)$, $\hat{B}(t)$, and $\hat{C}(t)$ read

$$\begin{aligned}
\hat{A}(t_1) &= e^{-i\frac{\pi}{4}\hat{J}_y} \cdot e^{i\hat{J}_z^2 t_1} \cdot e^{i\frac{\pi}{2}\hat{J}_y} \cdot e^{-i\hat{J}_z^2 t_1} \cdot e^{-i\frac{\pi}{4}\hat{J}_y}, \\
\hat{B}(t_2) &= e^{-i\frac{\pi}{4}\hat{J}_y} \cdot e^{-i\hat{J}_z^2 t_2} \cdot e^{i\frac{\pi}{2}\hat{J}_y} \cdot e^{i\hat{J}_z^2 t_2} \cdot e^{-i\frac{\pi}{4}\hat{J}_y}, \\
\hat{C}(t_3) &= e^{-i\frac{\pi}{4}\hat{J}_y} \cdot e^{-i\hat{J}_z^2 t_3} \cdot e^{i\frac{\pi}{2}\hat{J}_y} \cdot e^{i\hat{J}_z^2 t_3} \cdot e^{-i\frac{\pi}{4}\hat{J}_y}.
\end{aligned} \tag{2.2.3}$$

In the formula (2.2.2) the most important expressions are $\hat{A}$, $\hat{B}$ and $\hat{C}$ representing deformation. The other linear terms only compensate the deflection of the state around some of the axes, improving the overall performance of the emulated operator.
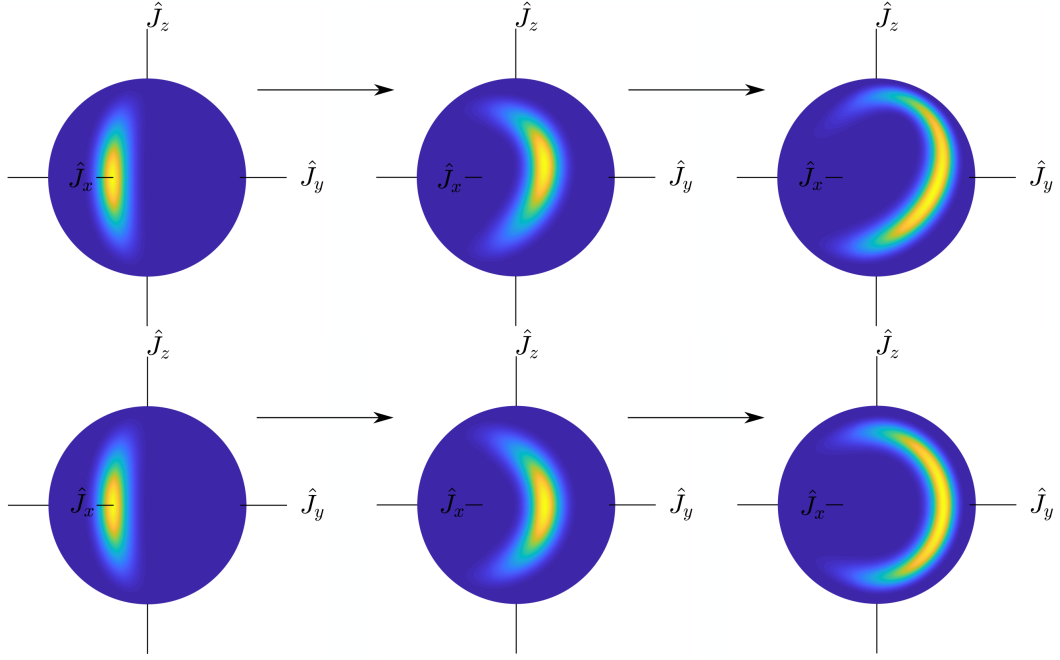
Figure II.1: Drawing of Q-function on the Bloch spheres. The first sphere in the first and second rows shows the initial compressed coherent state at which evolution is observed. The first row corresponds to the case where it is asymmetric (that is, imperfect breakdown given by the right side of the equation (2.1.7)) and the second row corresponds to the perfect case where asymmetry does not manifest (corresponds to perfect evolution, hence the left side of the equation (2.1.7)).

Chapter III

Numerical analysis

In the third chapter we analyze the performance of the preparation procedures from the previous chapter. To this end we employ numerical simulations and discuss the difficulty of finding global optimum of a non-convex function of eleven variables.

The analysis of the procedures was initially performed with coherent states; we used a cluster of 7 coherent states spatially restricted to 1.31% area of the Bloch sphere depicted in Fig. III.1. This cluster corresponds to a mixed state of 1.89 qubits in terms of von Neumann entropy

$$S = -\mathrm{tr}(\hat{\rho} \log_2 \hat{\rho}), \tag{3.0.1}$$

and improved on this by using squeezed coherent states instead. Consequently we reached 2.39 qubits with 6.5 dB of squeezing for a cluster of 7 states with 30% overlap between adjacent states. The spatial configuration of the cluster is depicted in Fig. III.1.
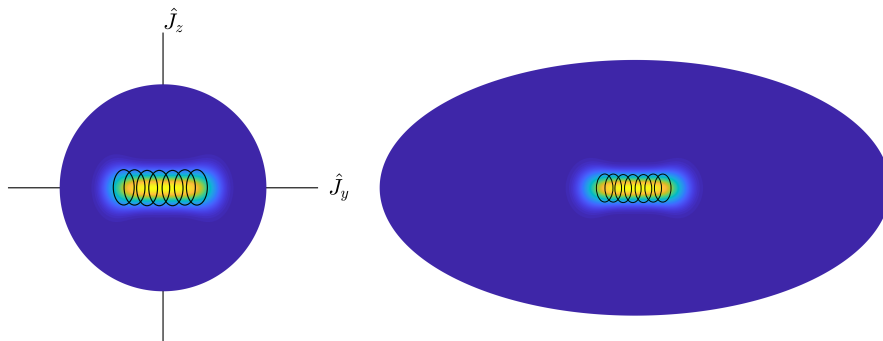

Figure III.1: The Bloch sphere covered by the Q-function is located in the left area of the image. The Bloch sphere in Hammer projection is covered with Q-function in the right part of the picture. Black ellipses highlight input compression states.

3.1 Functionality of the universal procedure

In Chapter II, we reviewed a method employing a sequence of commutators. We will now carry out a numerical analysis of the unitary evolution given by the formula (2.1.1) using all the necessary approximations and relations (2.1.6) — (2.1.9).

As a figure of merit we utilize fidelity, that is, the overlap

$$F = |\langle \psi | \phi \rangle|^2 \qquad (3.1.1)$$

between states $|\psi\rangle$ and $|\phi\rangle$

$$
\begin{aligned}
|\psi\rangle &= \hat{U}_{\text{cubic}}(\chi\tau) |\eta_0\rangle, & (3.1.2) \\
|\phi\rangle &= \hat{U}_{\text{universal}}(\chi\tau) |\eta_0\rangle, & (3.1.3)
\end{aligned}
$$

where $|\eta_0\rangle$ corresponds to a squeezed coherent state.

First we look at the functionality of the breakdown (2.1.10) using a linear and quadratic operator. We let this unitary operator evolve in time and compare it to the effects of exact cubic operator

$$
\begin{aligned}
\hat{U}_{\text{universal}}(\chi\tau) = {}& e^{\imath \hat{J}_x \frac{\pi}{2}} \cdot e^{-\imath \hat{J}_z^2 \chi\tau} \cdot e^{-\imath \hat{J}_x \frac{\pi}{2}} \cdot e^{\imath \hat{J}_y \frac{\pi}{2}} \cdot e^{imath \hat{J}_z^2 \chi\tau} \cdot e^{-\imath \hat{J}_y \frac{\pi}{2}} \cdot \\
& e^{-\imath \frac{\pi\sqrt{(2)}}{4}(\hat{J}_x - \hat{J}_y)} \cdot e^{-\imath (\hat{J}_z^2)\chi\tau} \cdot e^{\imath \frac{\pi\sqrt{(2)}}{4}(\hat{J}_x - \hat{J}_y)} \cdot \\
& e^{-\imath \frac{\pi\sqrt{(2)}}{4}(\hat{J}_x + \hat{J}_y)} \cdot e^{\imath (\hat{J}_z^2)\chi\tau} \cdot e^{\imath \frac{\pi\sqrt{(2)}}{4}(\hat{J}_x - \hat{J}_y)} \cdot \\
& e^{\imath \hat{J}_x \frac{\pi}{2}} \cdot e^{\imath \hat{J}_z^2 \chi\tau} \cdot e^{-\imath \hat{J}_x \frac{\pi}{2}} \cdot e^{\imath \hat{J}_y \frac{\pi}{2}} \cdot e^{-\imath \hat{J}_z^2 \chi\tau} \cdot e^{-\imath \hat{J}_y \frac{\pi}{2}} \cdot \\
& e^{-\imath \frac{\pi\sqrt{(2)}}{4}(\hat{J}_x - \hat{J}_y)} \cdot e^{\imath (\hat{J}_z^2)\chi\tau} \cdot e^{\imath \frac{\pi\sqrt{(2)}}{4}(\hat{J}_x - \hat{J}_y)} \cdot \\
& e^{-\imath \frac{\pi\sqrt{(2)}}{4}(\hat{J}_x + \hat{J}_y)} \cdot e^{-\imath (\hat{J}_z^2)\chi\tau} \cdot e^{\imath \frac{\pi\sqrt{(2)}}{4}(\hat{J}_x - \hat{J}_y)} \cdot \\
& e^{\imath \hat{J}_x \frac{\pi}{4}} \cdot e^{\imath \hat{J}_z^2 \chi\tau} \cdot e^{-\imath \hat{J}_x \frac{\pi}{4}} \cdot e^{-\imath \hat{J}_x \frac{\pi}{4}} \cdot e^{\imath \hat{J}_z^2 \chi\tau} \cdot e^{\imath \hat{J}_x \frac{\pi}{4}} \cdot \\
& e^{-\imath \hat{J}_y \frac{\pi}{4}} \cdot e^{-\imath \hat{J}_z^2 \chi\tau} \cdot e^{\imath \hat{J}_y \frac{\pi}{4}} \cdot e^{\imath \hat{J}_y \frac{\pi}{4}} \cdot e^{\imath \hat{J}_z^2 \chi\tau} \cdot e^{-\imath \hat{J}_y \frac{\pi}{4}} \cdot \\
& e^{\imath \hat{J}_x \frac{\pi}{4}} \cdot e^{\imath \hat{J}_z^2 \chi\tau} \cdot e^{-\imath \hat{J}_x \frac{\pi}{4}} \cdot e^{-\imath \hat{J}_x \frac{\pi}{4}} \cdot e^{-\imath \hat{J}_z^2 \chi\tau} \cdot e^{\imath \hat{J}_x \frac{\pi}{4}} \cdot \\
& e^{-\imath \hat{J}_y \frac{\pi}{4}} \cdot e^{\imath \hat{J}_z^2 \chi\tau} \cdot e^{\imath \hat{J}_y \frac{\pi}{4}} \cdot e^{\imath \hat{J}_y \frac{\pi}{4}} \cdot e^{-\imath \hat{J}_z^2 \chi\tau} \cdot e^{-\imath \hat{J}_y \frac{\pi}{4}} \cdot \\
& e^{\imath \frac{1}{4} \hat{J}_z \chi\tau}.
\end{aligned}
\qquad (3.1.4)
$$

In figure III.2 we observe that the fidelity drops rapidly to zero after a very short time and oscillates around zero. This is due to the expansion of (2.1.10) using linear and quadratic terms using formula (2.1.3) and the approximation (2.1.4). This causes asymmetric behavior and does not correspond to the exact cubic nonlinearity.

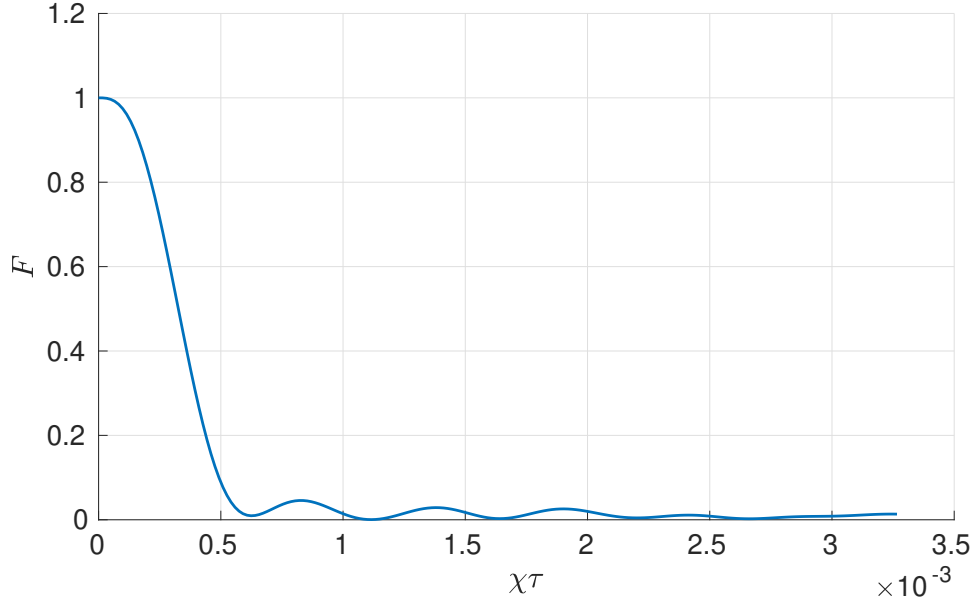However, this situation is not hopeless, there is a method we can use, namely the Suzuki-Trotter

Figure III.2: The plotted curve corresponds to the fidelity of the exact cubic operator and the universal procedure for $N = 60$ atoms.

decomposition, which is an important tool in numerical simulation and control of physical systems [27, 28].

The main idea of this method is that we repeatedly act on individual operators for a short period of time

$$\left(e^{\frac{\tau}{n}\hat{A}} \cdot e^{\frac{\tau}{n}\hat{B}}\right)^n = e^{\left(\hat{A}+\hat{B}\right)\tau} + \mathcal{O}\left(\frac{\tau^2}{n}\right) \tag{3.1.5}$$

Ideally, for an infinite number of iterations, the equtaion (3.1.5) becomes

$$\lim_{n\to\infty}\left(e^{\frac{\tau}{n}\hat{A}} \cdot e^{\frac{\tau}{n}\hat{B}}\right)^n = e^{\left(\hat{A}+\hat{B}\right)\tau} \tag{3.1.6}$$

The use of this method on equation (3.1.4) is shown using numerical simulation and subsequent plotting in figure III.3. We can see simulations made for different sized systems. An interesting thing that can be seen from this graph is that, with the number of atoms in the system increasing we need to increase the number of iterations of Suzuki-Trotter decomposition resulting in a greater number of steps to achieve fidelity of at least $F = 0.9$.

The figure III.4 shows the Q-function of the resultant states applied to the Bloch sphere (for all system sizes listed in the figure III.3) for 10 000 iterations of Suzuki-Trotter decomposition. Once we reach the systems sizes over 80 particles, a large number of iterations are needed (more than 10 000 iterations) and the state itself is not as well deformed as we would expect (the third and fourth lines of the figure III.4). Even 2000 iterations may be hard for the experiment because it would mean a sequence of larger quantities (corresponding to the number of individual unitary operators) of laser pulses.
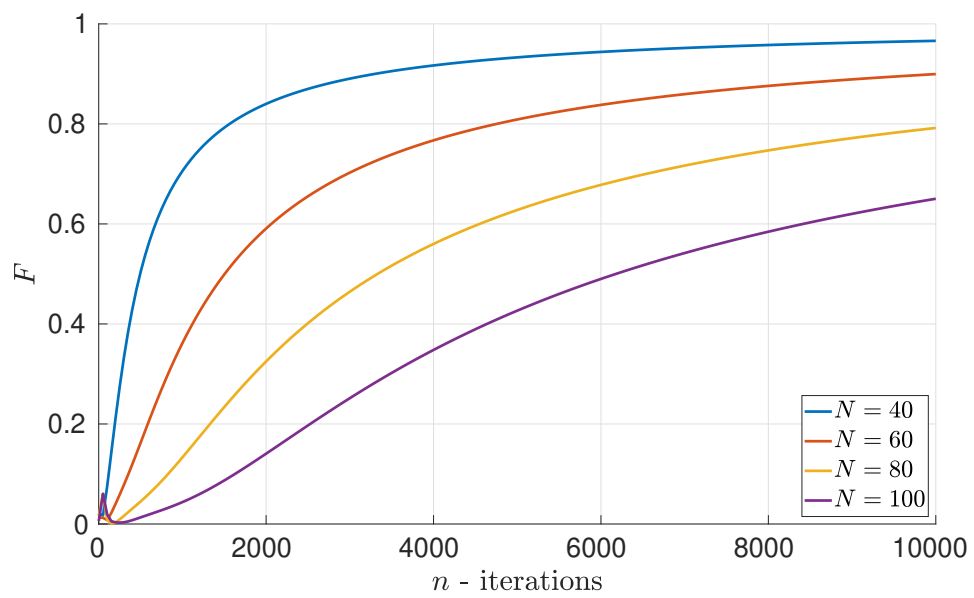
Figure III.3: Dependence of fidelity on the number of iterations of Suzuki-Trotter decomposition of the relation (2.1.1) for different numbers of particles N. The graph is plotted for a specific time $\chi\tau = \frac{\pi}{2\sqrt{N^3}}$.
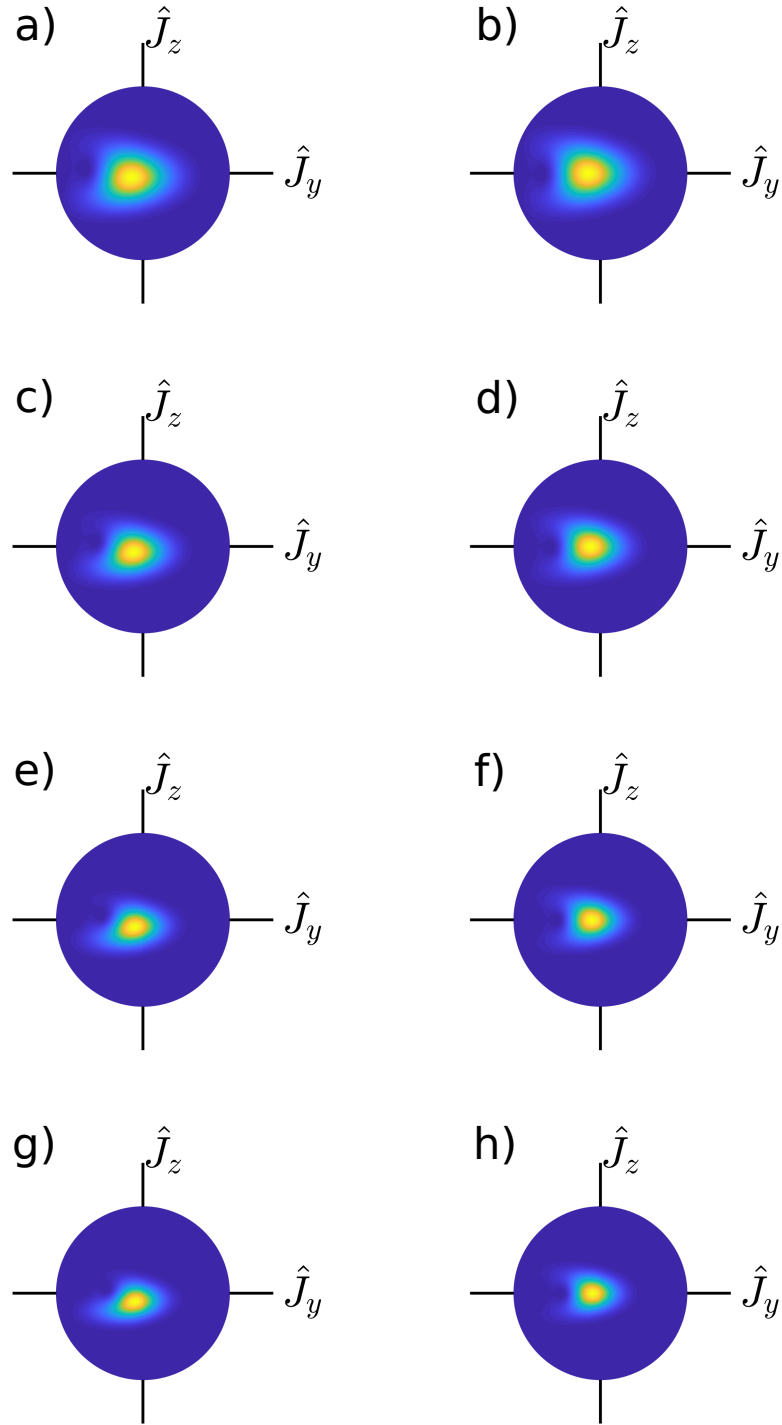
Figure III.4: Q-functions of individual states are shown on the Bloch sphere. The left block of the spheres shows the states created by the commutation method, and the right block shows the states created by the exact cubic Hamiltonian. The individual pairs of spheres correspond to a given number of atoms with value of fidelity: a), e) $N = 40$, $F = 0.97$; b), f) $N = 60$, $F = 0.90$; c), g) $N = 80$, $F = 0.79$; d), h) $N = 100$, $F = 0.65$. These correspond to the time of evolution $\chi\tau = \frac{\pi}{2\sqrt{N^3}}$ and the number of iterations $n = 10000$.

3.2 Functionality of the local procedure

Now we come to a more interesting part, namely to numerical analysis of the functionality of the local preparation procedure. This means verifying the functionality of the cubic operator (2.2.2) formed by the sequence of 23 operators. The problem with this approach, compared to the universal process, is that unlike in the universal case, we have no prior knowledge of the optimal values of the eleven parameters for $\hat{U}_{\text{local}}$ in (2.2.2) and have to find them numerically.

We optimize these eleven parameters to obtain the highest match with the exact cubic operator (2.1.5), that is to maximize the average fidelity

$$F = \frac{1}{n} \sum_{m=1}^{n} F_m, \tag{3.2.1}$$

where F_m are the fidelities of the n clustered states (in our case seven states) given by

$$F_m = |\langle \psi_m | \phi_m \rangle|^2. \tag{3.2.2}$$

The $|\psi_m\rangle$ and $|\phi_m\rangle$ are given as the evolution of the initial squeezed coherent states

$$
\begin{aligned}
|\psi_m\rangle &= \hat{U}_{\text{cubic}}(\chi\tau) |\eta_m\rangle, & (3.2.3) \\
|\phi_m\rangle &= \hat{U}_{\text{local}}(\alpha_1, \ldots, \alpha_8, t_1, t_2, t_3) |\eta_m\rangle, & (3.2.4) \\
|\eta_m\rangle &= e^{i\hat{J}_z\beta} |\eta_0\rangle, \quad \beta \in \langle -\pi, \pi \rangle, & (3.2.5)
\end{aligned}
$$

with $|\eta_0\rangle$ representing the squeezed coherent state.

3.2.1 Optimization

The fidelity (3.2.1) is a function of 11 variables — t_1, t_2, t_3, $\alpha_1, \ldots, \alpha_8$ — appearing in emulating operator (2.2.2). In order to find a global maximum of this function we need to investigate its properties and choose an appropriate optimization method.

Following the axial restrictions of (3.2.1), depicted in the Figure III.5, we quickly conclude that (3.2.1) is not a convex function. We can also observe oscillatory behaviour in t_1, t_2 and t_3 variables.

Since we are dealing with a non-convex problem we are unable to get away with a simple local optimization; instead we must choose a different, global approach. We uniformly sample the parametric space and perform local optimization from different starting points, making use of an unconstrained quasi-Newtonian method implemented in the standard library function `fminunc` of the `MATLAB` software suite [29] with BFGS [30, 31] method used to calculate the matrix of second derivatives of the objective function (3.2.1).
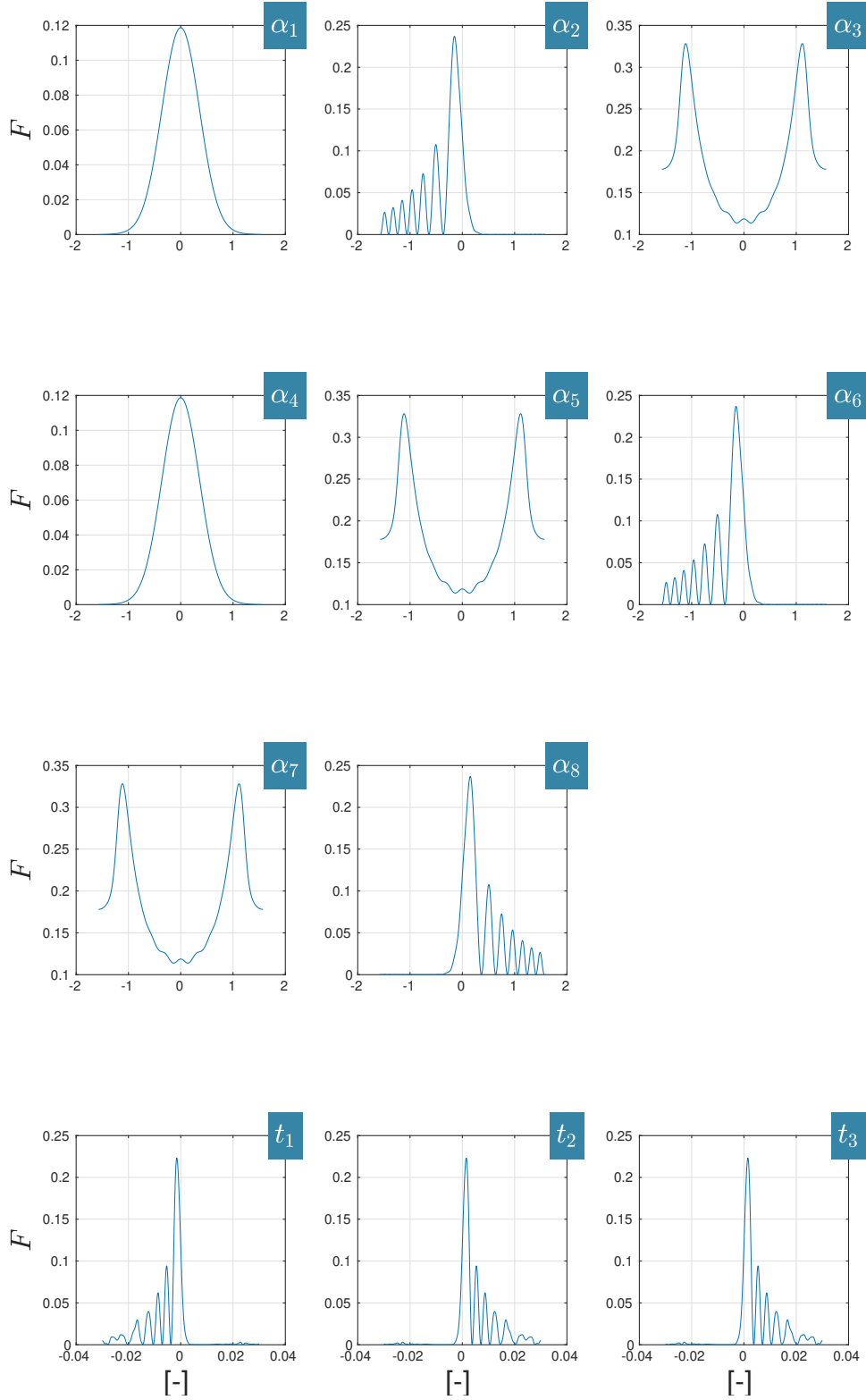
Figure III.5: Potential of parameters. Parameters α_1 - α_8 correspond to rotation angles of linear operators 1.2.1 and parameters t_1, t_2 and t_3 are time parameters of quadratic operator 1.2.4. In each plot only a single parameter is varied while all the other parameters are fixed to the zero values.

The results obtained by utilizing this optimization strategy are presented in Fig. III.6 (potential of optimized parameters for $\chi\tau = 2.7 \cdot 10^{-3}$ is shown in the figure III.7). We show the fidelity of the local, optimized strategy (in red), the universal strategy with 5000 iterations (in blue) and with no interaction whatsoever (yellow). The fidelity is calculated with respect to the ideal cubic interaction.
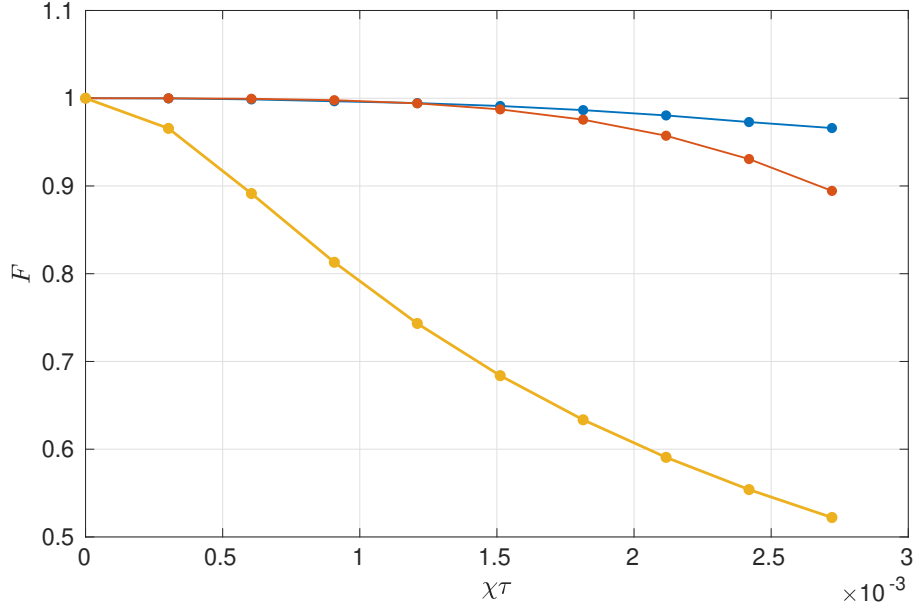

Figure III.6: Figure of results after optimization. We see 3 curves with points, points correspond to individual samples of the simulation. The yellow curve corresponds to when we do nothing with the initial state, red corresponds to the universal procedure with 5000 iterations and blue corresponds to the local optimized procedure.

There are only 10 optimized points in Fig. III.6 due to computation complexity. The simulation was performed for $N = 60$ particles; we used 300 random samples of parameters to find the global optimum in each of the 10 points. Even though we performed the underlying local optimization in parallel each point took over 30 minutes on average to calculate.

While the optimal fidelity is well behaved the optimal parameters vary rapidly between adjacent points; rendering continous interpolation impossible. Since we need to know the parameters at any given time we are forced to address this issue. Fortunately we have several options.

The first option is to optimize for each infinitesimal point of the time continuum. This is time consuming and, since the parameters change rapidly, ineffective and experimentally infeasible. The second option is to fix the optimal parameters between discrete points. As it turns out this is not the brightest idea. In the third approach we perform further local optimization starting from the globally optimal points. For the sake of simplicity we utilize a steepest descent method, following the numerically calculated gradient of (3.2.1).

These three options are discussed in Fig. III.8. It is clear that naively fixing the parameters (the second option) performs poorly. In contrast the steepest descent starting from global optima (third option) performs rater well.
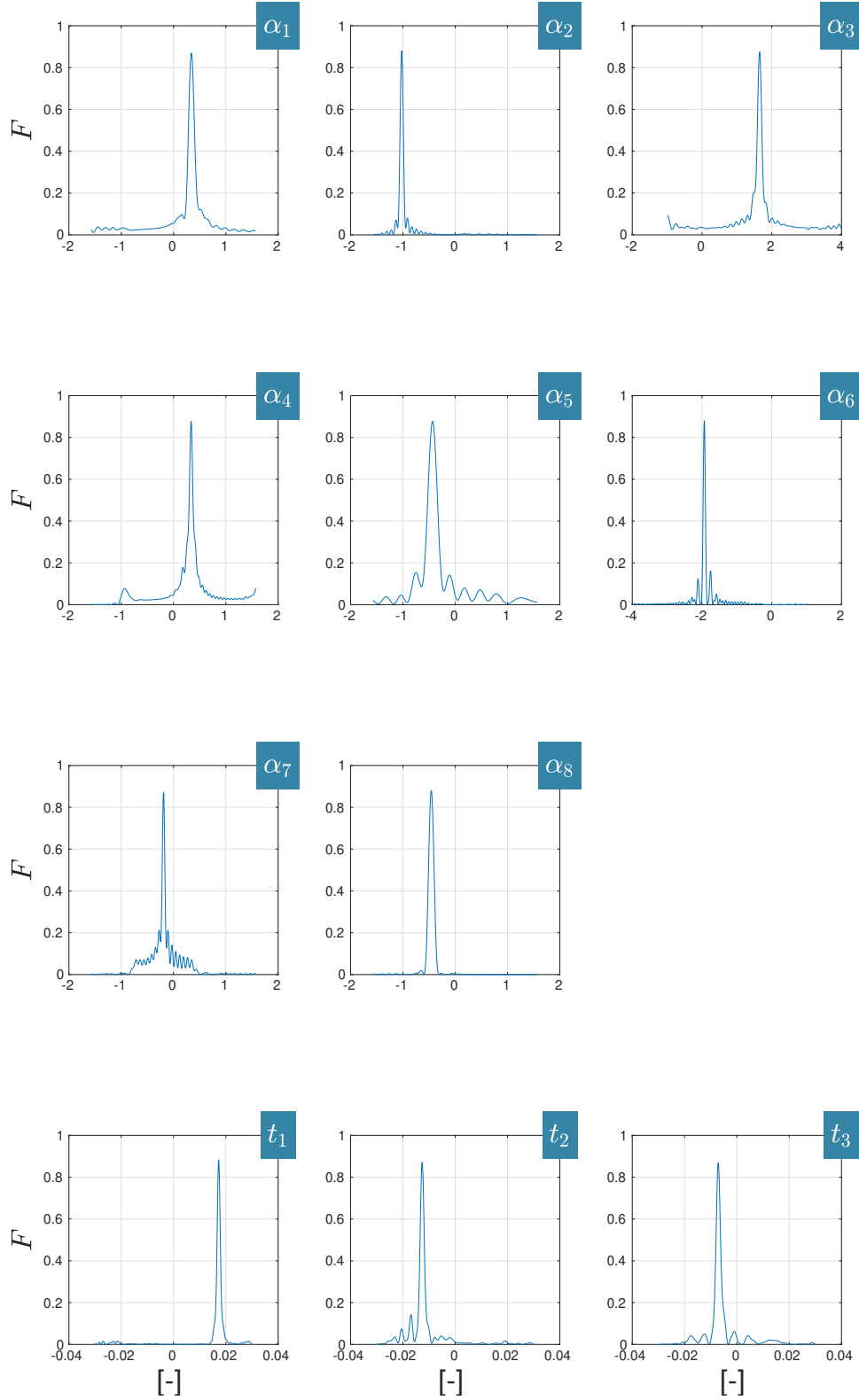
Figure III.7: Potential of optimized parameters for $\chi\tau = 2.7 \cdot 10^{-3}$. Parameters α_1 - α_8 correspond to rotation angles of linear operators 1.2.1 and parameters t_1, t_2 and t_3 are time parameters of quadratic operator 1.2.4. In each plot only a single parameter is varied while all the other parameters are fixed to their optimal values.
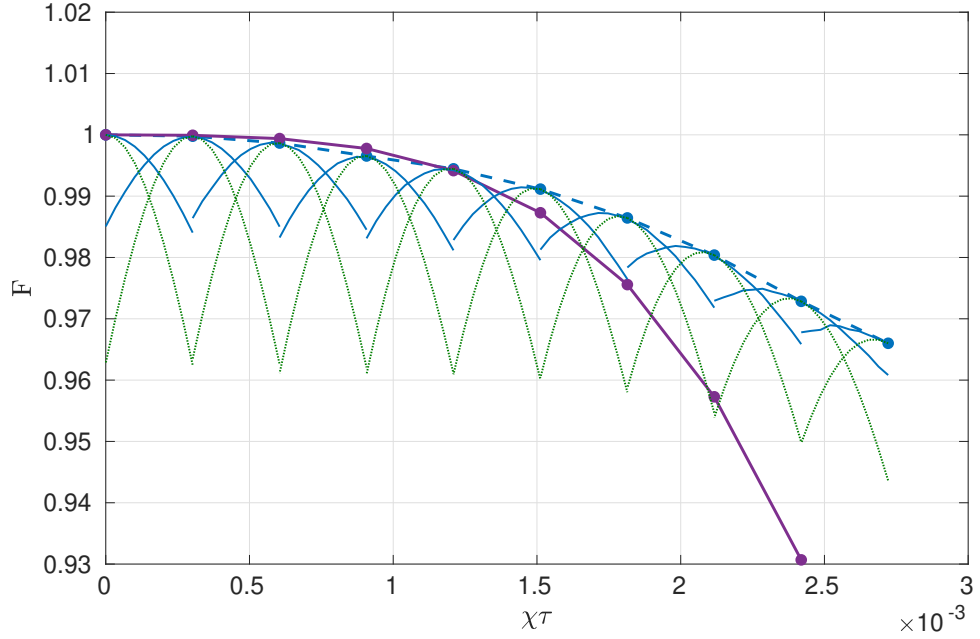
Figure III.8: Figure of results after the second (numerical gradient) optimization. We see few curves, let start with the purple one, this curve corresponds to the universal procedure (2.1.10) using the Suzuki-Trotter decomposition (5000 iterations), the second one is the blue dashed curve corespond to the local procedure (2.2.2) optimized by BFGS optimizetion, the third curves are green and they corespond to using optimized parameters (ten time samples) for a wider range of times (based on only one optimization) and last curves - blue full curves, coresponds to numerical gradient optimization based on optimized points obtained by BFGS optimization.

3.2.2 Optimization functionality

We managed to optimize parameters to create a cubic operator quite well. We reach fidelity up to $F = 0.97$ for the effective interaction time $\chi\tau = 2.7 \cdot 10^{-3}$. The question is how well this optimization works. We did this optimization for only seven states and we are interested in knowing how our optimized formula works on the entire Bloch sphere. While our procedure works with squeezed states we decided to use coherent states because there would otherwise be issues with problem of ambiguity of the orientaton of the squeezed states at the poles

pole coverage and orientation of squeezed states. The sphere was covered with 80 000 coherent states. First, we observed the evolution of these states due to the exact (3.2.3) cubic operator. We then calculated fidelity (overlap) with states that were affected by the optimized operator sequence (3.2.4).

Figure III.9 shows the functionality of our optimized formula. The fidelity of the procedure is displayed on Block sphere in Hammer's projection. In the picture the ellipse highlighted by the dashed black line represents the area for which the optimization was performed, that is, our seven coherent states. This area corresponds to 1.31% of the whole Bloch sphere. We can see that over time, the functional area is getting smaller. We begin by covering the entire sphere

(which is logical for the time of cubic deformation $\chi\tau = 0$, when there is no change in the state), to the area that corresponds to 7% of the total area of the Bloch sphere (for cubic deformation $\chi\tau = 2.7 \cdot 10^{-3}$). The size of the area was determined by the boundary fidelity $F = 0.8$, when $F < 0.8$ does not belong to the calculated area, when $F > 0.8$ this area is included. For the demonstration we chose four different values of the time, to see how much the area of functionality changes, these spheres (figure III.9 row two and row three) corresponding to cubic deformation for values of the time $\chi\tau = 0.6 \cdot 10^{-3}$ and $\chi\tau = 1.8 \cdot 10^{-3}$. We explain why the area is diminishing by the fact that with the increasing time of cubic deformation, the demand for asymmetry we use is growing of the time. However, we get this asymmetry maximally in the area from the $\hat{J}_x$ axis in the range $-\frac{\pi}{2}$ to $\frac{\pi}{2}$ then somewhat different deformations occur, which are not useful to us for cubic deformation. This would be the functionality of the optimized sequence (2.2.2) on the bloch sphere full of coherent states. Now comes the next thing we would like to verify. It is the robustness of optimized parameters to change the size of the system (change of the number of particles N).
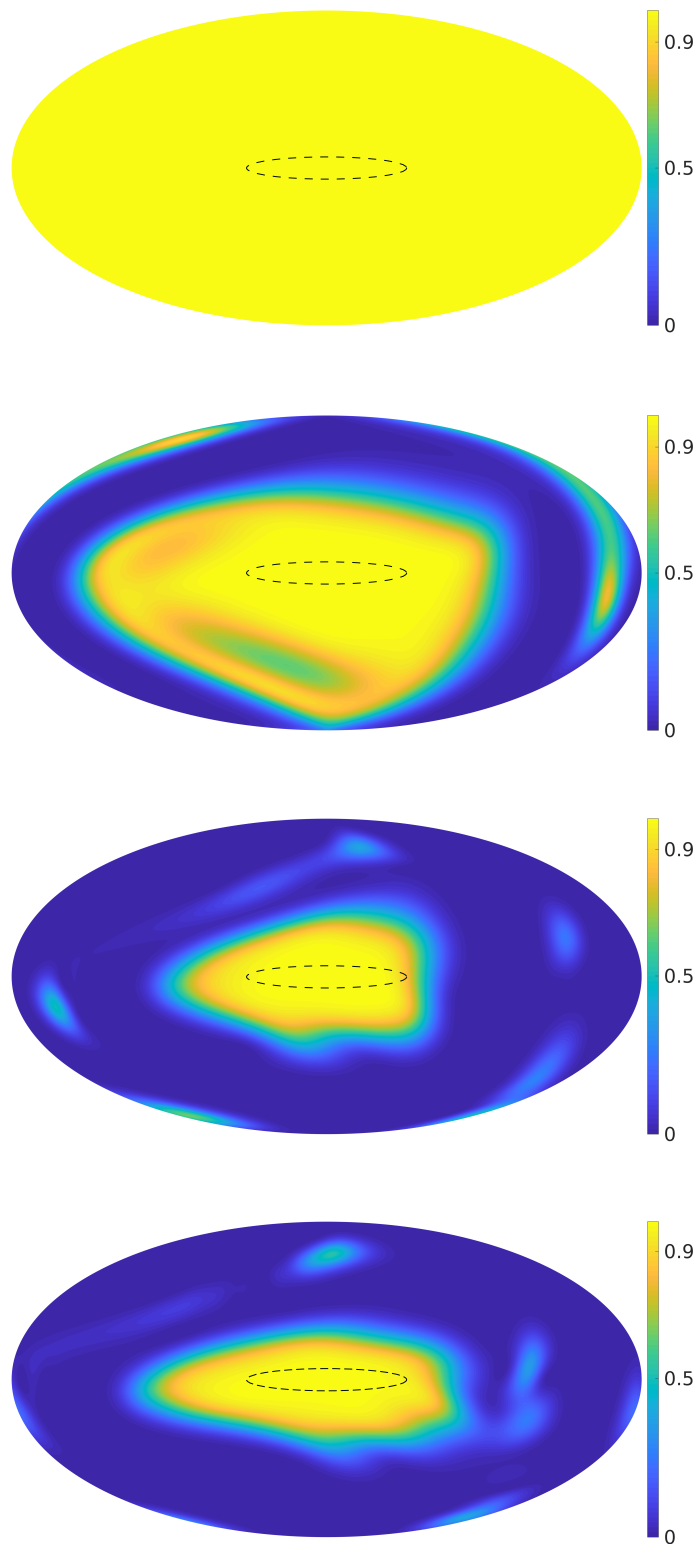
Figure III.9: Projection of fidelity on the Bloch sphere. The black highlighted ellipse indicates the optimized area. The first sphere (first row) corresponds to cubic deformation for $\chi\tau = 0$ and the last sphere (last row) corresponds to cubic deformation for $\chi\tau = 2.7 \cdot 10^{-3}$.

3.2.3   Robustness with respect to unknown atome numbers

One of the things we want to determine is the robustness of optimized parameters in respect to change of the number of particles in the system. Once our procedure becomes experimentally feasible, the exact number of particles may not be known as the exact number of atoms in the system might have Poissonian distribution and fluctuate around N accuracy of $\pm\sqrt{N}$.

We use our optimized formula and map it to systems with numbers of atoms up to $\pm\sqrt{N}$. A numerical simulation was performed where we had an optimized formula for $N = 100$ (to get an integer from the square root) and the maximum time $\chi\tau = 1.26 \cdot 10^{-3}$ of cubic deformation corresponds to the maximum time $t = 2.7 \cdot 10^{-3}$ of cubic deformation for $N = 60$ atoms. The results are shown in the figure III.10.
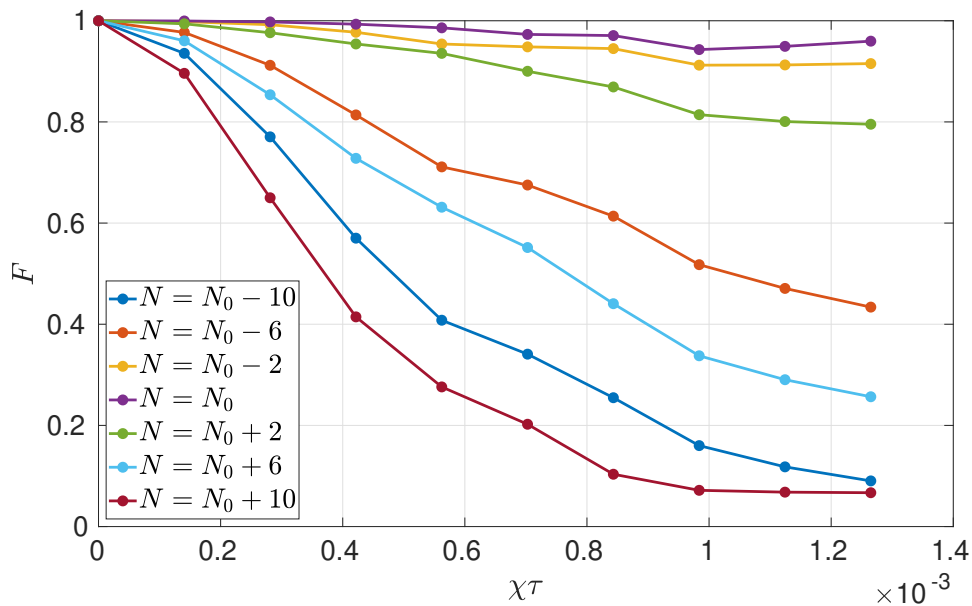

Figure III.10: The change of fidelity depending on the number of particles in the system. The parameters used to analyze robustness where local procedure is optimized for $N_0 = 100$. The points in the figure correspond to tested samples.

In the figure III.10, we can see that fidelity, for almost all system sizes except for the optimized $N = 100$, falls below $F = 0.8$ and in some cases ($N = 90$, $N = 110$) even below $F = 0.2$. Fidelity decreases with every added or removed particles. The question is, what is the cause of this problem. It is possible that the optimization method is improperly chosen or the whole local procedure formula is inappropriate. One way is to look at what the resulting states look like and how they should look like (let's show only extreme cases and optimized, that is, when $N = 90$, $N = 100$, $N = 110$). We use squeezed coherent states and act on them both by the exact cubic operator and the optimized ones and draw their Q-function on the Bloch sphere, and consequently it becomes more readable where the problem arises.
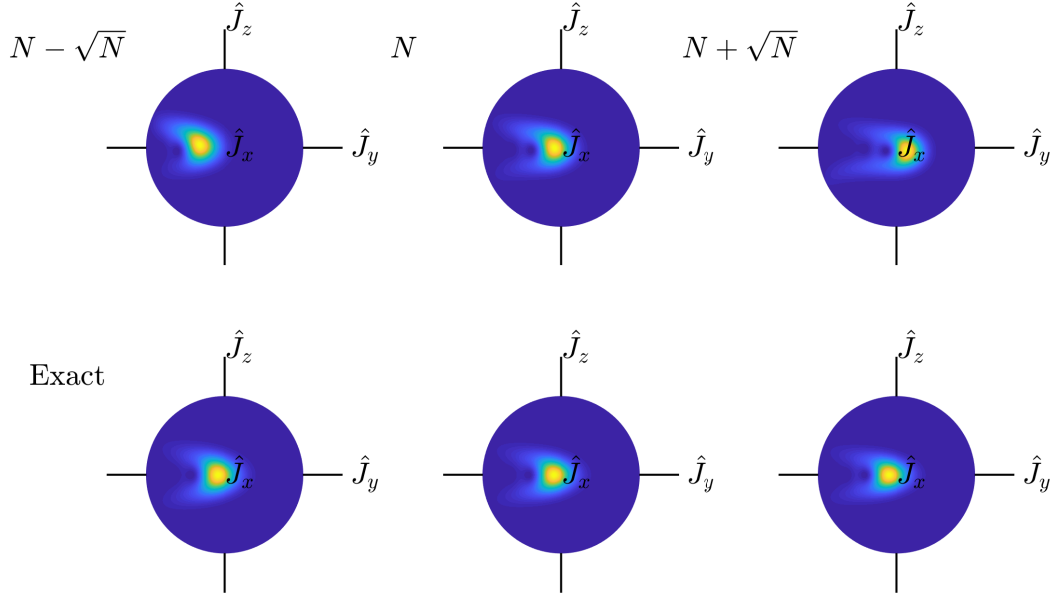
Figure III.11: Bloch spheres with result states (Q-function). In the first row, we can see the results using an optimized local method that is optimized for a particular N and we use it for $N + \sqrt{N}$ and $N - \sqrt{N}$. In the second row we can see the exact case for N, $N + \sqrt{N}$ and $N - \sqrt{N}$, where $N = 100$.

If we look at the figure III.11 of the first row in the first and the third sphere, we can see that cubic deformation occurs in systems of sizes $N = 90$ and $N = 110$, but the states are more deflected from the $\hat{J}_x$-axis than after the exact cubic deformation (second row of the figure III.11). There are several ways to solve this problem.

Our first solution is based on the application of a linear operator. This operator, with a correctly selected rotation angle γ, rotates the state to the correct position and thus obtains a higher fidelity. To get an idea of how the deviation angle γ changes on the size of the system, we have simulated a wider particle count range $N = \langle 86, 114 \rangle$ for one particular time $\chi \tau = \frac{\pi}{2\sqrt{N^3}}$. We performed fit, in the MATLAB program, on the obtained data by numerical simulation (the figure III.12). Second-order polynomial function was used to fit the simulated values

$$\gamma(N) = p_1 \cdot N^2 + p_2 \cdot N + p_3, \tag{3.2.6}$$

when the p_i parameters were obtained by the MATLAB and have these values

$$
\begin{aligned}
p_1 &= 2.212 \cdot 10^{-4}, \\
p_2 &= -6.501 \cdot 10^{-2}, \\
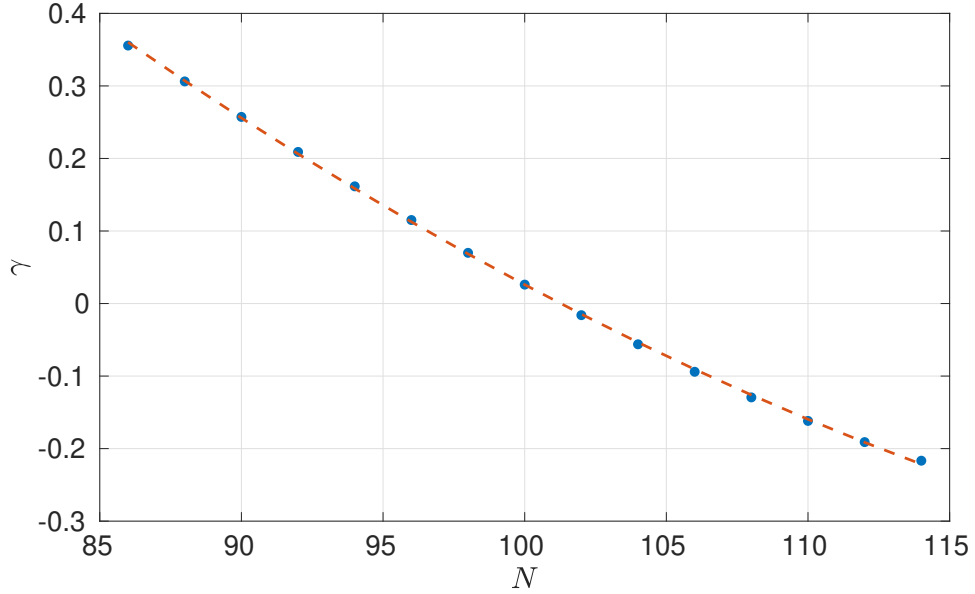p_3 &= 4.315.
\end{aligned}
\tag{3.2.7}
$$

Figure III.12: Fit on simulated data. Dependence of the γ rotation parameter on the number of particles N in the system.

When we apply a linear operator (1.2.1) with the correct value of the γ parameter to the resulting state, the fidelity is increased in the case of $N = 110$ atoms from $F = 0.06$ to $F = 0.80$ (the difference with and without rotation is shown in Figure III.13). The gamma angle was calculated for all time cases shown in the figure III.10 and the results are shown in the figure III.14.
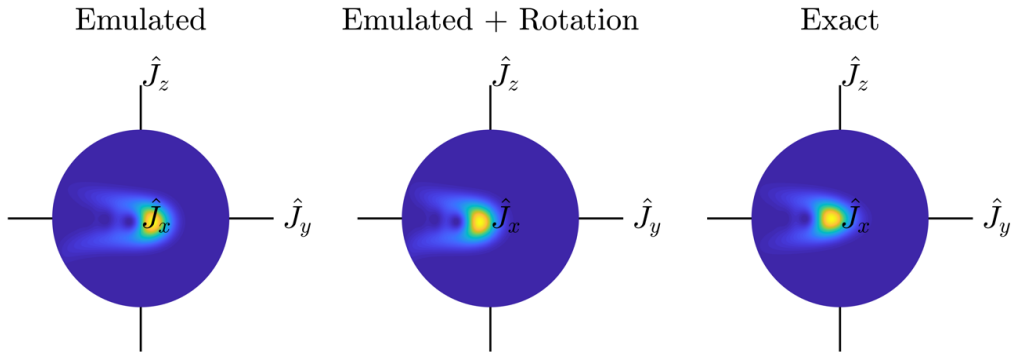

Figure III.13: A representation of what the compensation using a linear operator. This example is directly for $N = 110$ when a local procedure is optimized for $N = 100$. The left two spheres correspond to the local procedure (in this order: local procedure, local procedure + compensation) and the right sphere corresponds to the exact case for $N = 110$.

When we look at the resulting figure III.14 of fidelity after the rotation compensation, we can see that fidelity even for extreme cases of the number of particles of the system has increased quite a bit and does not get below the limit of $F = 0.8$.
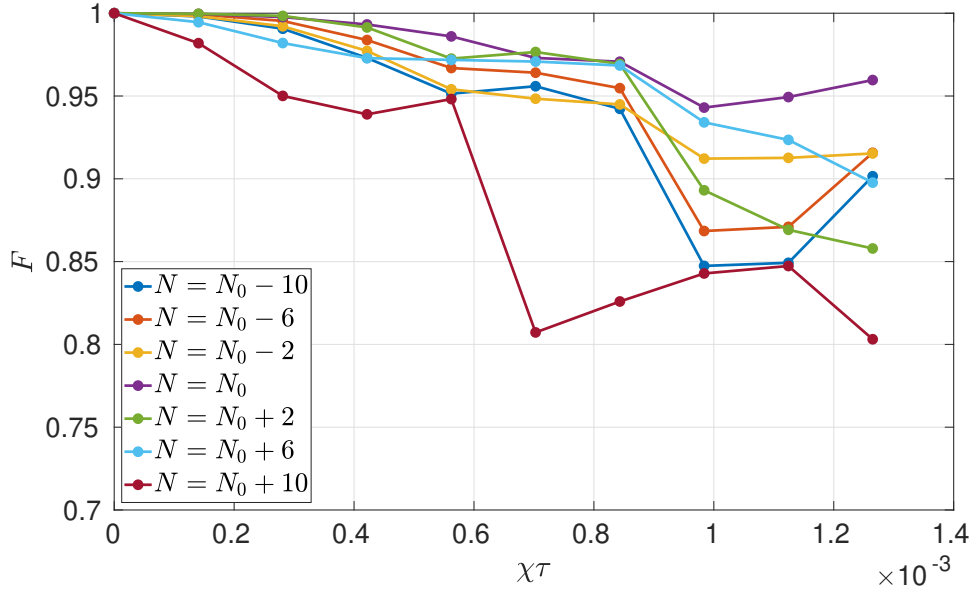
Figure III.14: The change of fidelity depending on the number of particles in the system, for $N_0 = 100$. in this case, the resulting state deflection is compensated by the rotation (linear operator (1.2.1)).

Another way to improve fidelity for different sized systems is to adjust the optimization itself. It means to adjust the condition that we optimize, to include both fidelity and boundary possibilities, ie in our case for $N = 90$ and $N = 110$. The optimized expression reads

$$F_{\text{all}} = F_{90} + F_{100} + F_{110}. \tag{3.2.8}$$

instead of (3.2.1).

Therefore, if we optimize (3.2.8), we achieve relatively high fidelity, the results are shown in figures III.15 and III.16. The fidelity does not get below $F = 0.89$ after the new optimization, but the problem is the difficulty of optimization and its long duration. Instead of 10 time points, we optimized in 5, with this optimization taking 3 times longer than in the cases mentioned in the section 3.2.1.
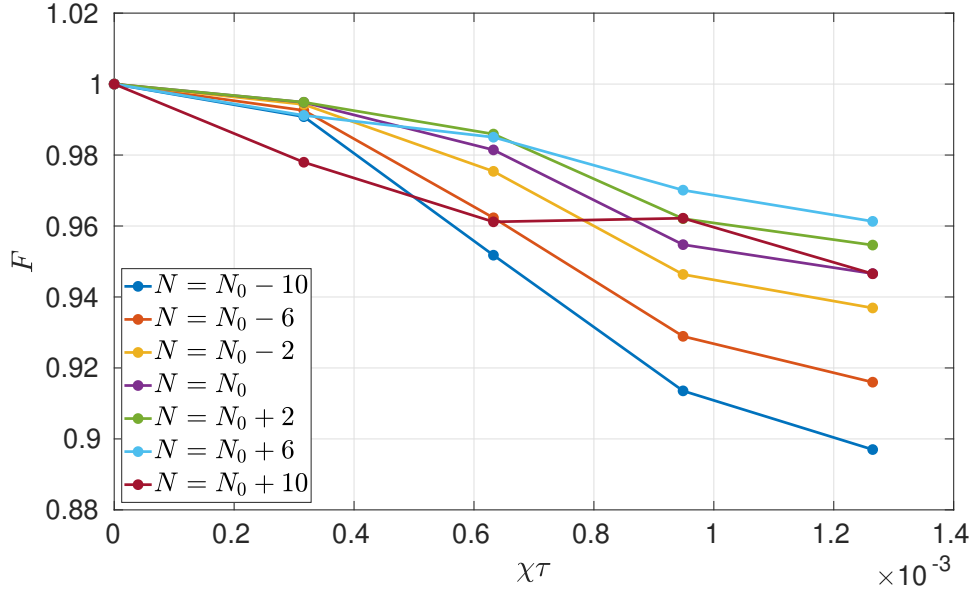
Figure III.15: The change of fidelity depending on the number of particles in the system, where $N_0 = 100$. In this case is local procedure optimized for wider interval for different number of particles as opposed to figure III.10.
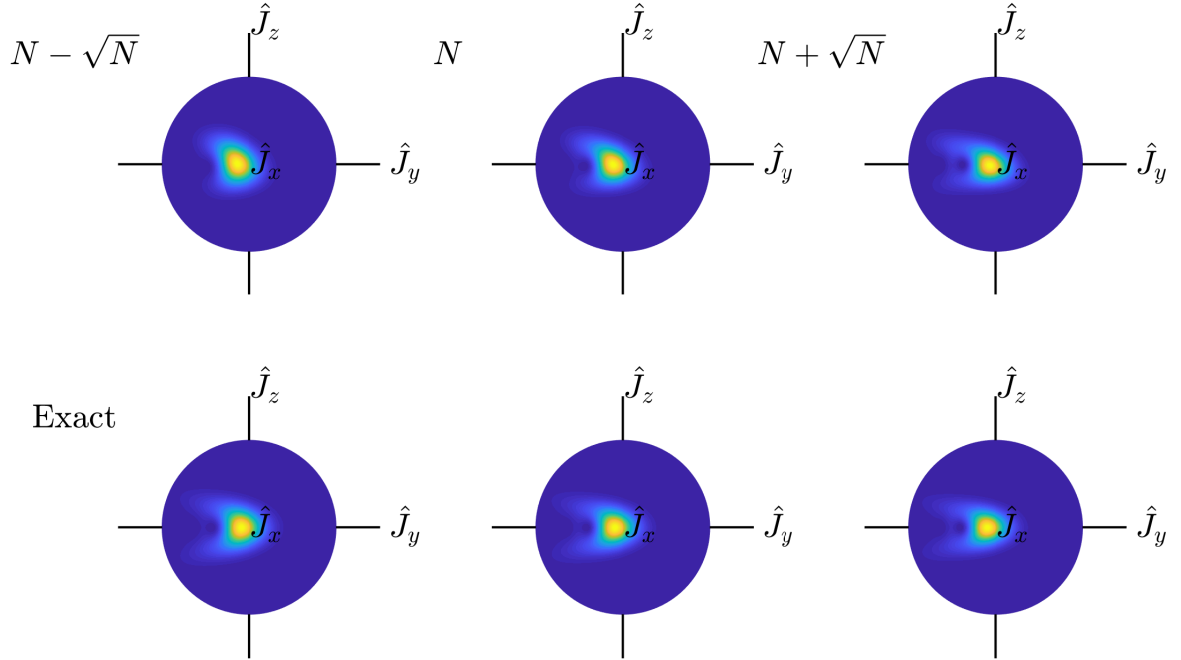

Figure III.16: Bloch spheres with result states (Q-function). In the first row, we can see the results using an optimized local method that is optimized for for wider interval for different number of particles. In the second row we can see the exact case for N, $N + \sqrt{N}$ and $N - \sqrt{N}$, where $N = 100$.

Conclusion and outlooks

The aim of this work was to find a way of creating a cubic operator of collective spin system in the simplest possible way. We started with the derived formula (2.1.1), which was based on commutation identities. Theoretically we should get an operator identical to the exact cubic operator. Our further motivation was to create a cubic operator that could be realized experimentally, that is, only using operators that can be accessed in a contemporary laboratory settings. This meant taking formula (2.1.1) and breaking it down to (1.2.1) and (1.2.4) operators. Due to this approximative process our formula corresponded to the exact cubic operator only for short time periods. For longer times the fidelity with the exact operator fell quite low. It was necessary to perform a numerical analysis of the approximative formula. During the analysis, we encountered one term that was asymmetrical and later turned out to be useful in alternative construction of a cubic operator. To reduce the error caused by approximations and to reduce the asymmetry of the behavior of individual terms, we used Suzuki-Trotter decomposition, which led to the resolution of our problems, but only in the numerical sense as it was necessary to make thousands of iterations of the formulua (3.1.4). In essence this would mean a sequence of a larger number of laser pulses, complexity of which would be prohibitive in experimental setting.

As was mentioned, we encountered a term that exhibited unsymmetrical behavior in the numerical analysis of individual parts of the formula (2.1.1). By using this term and sequences of other linear and quadratic operators, we were able to create a formula behaving like an exact cubic operator.

However, we ecountered a problem while analyzing our formula of a local processes for different times. The procedure had to be optimized for each time step and we had to optimize a function of 11 parameters. To determine the optimization method we looked at the shape of the optimized function in respect to the individual parameters. After considering its behaviour we decided to employ quasi-Newtonian optimization with BFGS Hessian approximation method and a simple globalization strategy.

After successful optimization, it was necessary to determine the efficiency of the local procedure. Our procedure was optimized for 7 coherent states covering roughly 1.31% of Bloch's sphere. We analyzed the area of the sphere where we got fidelity $F > 0.8$ and found it to be roughly 7%, which is about five times the area we have optimized for.

The last part of this work was to analyze the robustness of the parameters depending on the size of the system, that is how robust procedure is if we optimize its paremeters for a certain system size, for example $N = 100$ and then use these parameters for a system with $N = 110$ particles.

It turned out that with the increasing system size the fidelity rapidly decreases and after visualising the resulting states on the Bloch sphere we saw that the deformation still corresponded to the cubic deformation, but that the state was deflected. Therefore, we introduced compensation by linear operator, essentially performing a rotation and obtained, for the most extreme cases such as $N = 90$ increase of fidelity from $F = 0.09$ to $F = 0.9$.

The second option that we considered was updating the original optimization and modifying to account for different numbers of particles. For the $N = \left[N_0 - \sqrt{N_0}, N_0 + \sqrt{N_0}\right]$ interval with $N_0 = 100$ we found out the fidelity does not fall below $F = 0.89$. However, the time complexity of the optimization increased significantly.

To sum up, we have managed to create a cubic operator using a sequence of 23 linear and quadratic operators that can be implemented in laboratory setting. We reached fidelity $F = 0.97$ for the time $\chi\tau = 2.7 \cdot 10^{-3}$ for $N = 60$, and $F = 0.96$ for the time $\chi\tau = 1.26 \cdot 10^{-3}$ for $N = 100$. We have accomplished the goals we set in the beginning, that is we achieve J_z^3 in relatively few iterations. We hope our method will be, in time, realized experimentally. In the future we would like to use this relatively simple approach to construct higher order operators.

Bibliography

[1] Feynman, R. P. "Simulating physics with computers". In: *International Journal of Theoretical Physics* 21.6-7 (June 1982), pp. 467–488. URL: https://doi.org/10.1007/bf02650179.

[2] Ulmann, B. *Analog computing.* Walter de Gruyter, 2013.

[3] *Analogical models.* Sept. 2017. URL: https://en.wikipedia.org/wiki/Analogical_models.

[4] E. Grumbling and M. Horowitz, eds. *Quantum Computing.* National Academies Press, Mar. 2019. URL: https://doi.org/10.17226/25196.

[5] Braunstein, S. L. and Loock, P. van. "Quantum information with continuous variables". In: *Reviews of Modern Physics* 77.2 (June 2005), pp. 513–577. URL: https://doi.org/10.1103/revmodphys.77.513.

[6] Weedbrook, C., Pirandola, S., García-Patrón, R., Cerf, N. J., Ralph, T. C., Shapiro, J. H., and Lloyd, S. "Gaussian quantum information". In: *Reviews of Modern Physics* 84.2 (May 2012), pp. 621–669. URL: https://doi.org/10.1103/revmodphys.84.621.

[7] Lloyd, S. and Braunstein, S. L. "Quantum Computation over Continuous Variables". In: *Physical Review Letters* 82.8 (Feb. 1999), pp. 1784–1787. URL: https://doi.org/10.1103/physrevlett.82.1784.

[8] Deutsch, D. "Quantum theory, the Church–Turing principle and the universal quantum computer". In: *Proceedings of the Royal Society of London. A. Mathematical and Physical Sciences* 400.1818 (1985), pp. 97–117.

[9] Sakurai, J. J. *Modern quantum mechanics.* Addison-Wesley Pub. Co, 1994. ISBN: 0-201-53929-2.

[10] Ma, J., Wang, X., Sun, C., and Nori, F. "Quantum spin squeezing". In: *Physics Reports* 509.2-3 (Dec. 2011), pp. 89–165. URL: https://doi.org/10.1016/j.physrep.2011.08.003.

[11] Opatrný, T. "Squeezing with classical Hamiltonians". In: *Physical Review A* 92.3 (Sept. 2015). URL: https://doi.org/10.1103/physreva.92.033801.

[12] Kitagawa, M. and Ueda, M. "Squeezed spin states". In: *Phys. Rev. A* 47 (6 June 1993), pp. 5138–5143. URL: https://link.aps.org/doi/10.1103/PhysRevA.47.5138.

[13] Leroux, I. D., Schleier-Smith, M. H., and Vuletić, V. "Implementation of Cavity Squeezing of a Collective Atomic Spin". In: *Physical Review Letters* 104.7 (Feb. 2010). URL: `https://doi.org/10.1103/physrevlett.104.073602`.

[14] Schleier-Smith, M. H., Leroux, I. D., and Vuletić, V. "Squeezing the collective spin of a dilute atomic ensemble by cavity feedback". In: *Physical Review A* 81.2 (Feb. 2010). URL: `https://doi.org/10.1103/physreva.81.021804`.

[15] Condon, E. *The theory of atomic spectra*. Cambridge: Cambridge University Press, 1951. ISBN: 978-0-521-09209-8.

[16] T. Opatrný, M. K. and Das, K. K. "Spin squeezing by tensor twisting and Lipkin-Meshkov-Glick dynamics in a toroidal Bose-Einstein condensate with spatially modulated nonlinearity". In: *Phys. Rev. A* 91 (5 May 2015), p. 053612. URL: `https://link.aps.org/doi/10.1103/PhysRevA.91.053612`.

[17] Opatrný, T. "Twisting tensor and spin squeezing". In: *Phys. Rev. A* 91 (5 May 2015), p. 053826. URL: `https://link.aps.org/doi/10.1103/PhysRevA.91.053826`.

[18] Estève, J., Gross, C., Weller, A., Giovanazzi, S., and Oberthaler, M. K. "Squeezing and entanglement in a Bose–Einstein condensate". In: *Nature* 455.7217 (Oct. 2008), pp. 1216–1219. URL: `https://doi.org/10.1038/nature07332`.

[19] Dicke, R. H. "Coherence in Spontaneous Radiation Processes". In: *Phys. Rev.* 93 (1 Jan. 1954), pp. 99–110. URL: `https://link.aps.org/doi/10.1103/PhysRev.93.99`.

[20] Liu, W.-F. and Hu, Z.-D. *Constructions of Dicke states in high spin multi-particle systems*. 2015. eprint: `arXiv:1511.03281`.

[21] Radcliffe, J. M. "Some properties of coherent spin states". In: *Journal of Physics A: General Physics* 4.3 (May 1971), pp. 313–323. URL: `https://doi.org/10.1088%2F0305-4470%2F4%2F3%2F009`.

[22] Leonhardt, U. *Essential Quantum Optics*. Cambridge University Press, 2009. URL: `https://doi.org/10.1017/cbo9780511806117`.

[23] Nielsen, M. *Quantum computation and quantum information*. Cambridge New York: Cambridge University Press, 2010. ISBN: 9781107002173.

[24] Snyder, J. *Flattening the earth : two thousand years of map projections*. Chicago: University of Chicago Press, 1993. ISBN: 0-226-76747-7.

[25] Husimi, K. "Some Formal Properties of the Density Matrix". In: *Proceedings of the Physico-Mathematical Society of Japan. 3rd Series* 22.4 (1940), pp. 264–314.

[26] Opatrný, T. "Quasicontinuous-Variable Quantum Computation with Collective Spins in Multipath Interferometers". In: *Physical Review Letters* 119.1 (July 2017). URL: `https://doi.org/10.1103/physrevlett.119.010502`.

[27] Hatano, N. and Suzuki, M. "Finding Exponential Product Formulas of Higher Orders". In: *Quantum Annealing and Other Optimization Methods*. Springer Berlin Heidelberg, Nov. 2005, pp. 37–68. URL: `https://doi.org/10.1007/11526216_2`.

[28] Dhand, I. and Sanders, B. C. "Stability of the Trotter-Suzuki decomposition". In: *Journal of Physics A: Mathematical and Theoretical* 47.26 (June 2014), p. 265206. URL: `https://doi.org/10.1088/1751-8113/47/26/265206`.

[29] MathWorks. *Find minimum of unconstrained multivariable function - matlab*. URL: https://www.mathworks.com/help/optim/ug/fminunc.html (visited on 04/25/2010).

[30] J. Machalová, H. N. *Numerické metody nepodmíněné optimalizace*. Vol. 1. Univerzita Palackého v Olomouci, 2013. ISBN: 978-80-244-3403-2.

[31] Dai, Y.-H. *A perfect example for the BFGS Method*. URL: ftp://www.cc.ac.cn/pub/dyh/papers/bfgs-example.pdf (visited on 04/25/2010).